SPIE Conf. Proc.: Smart Structures and Materials 2005: Active Materials: Behavior and Mechanics, March, 2005, San Diego, CA

Properties and Potential of Two (Ni,Pt)Ti Alloys for Use as High-Temperature Actuator Materials

Ronald Noebe[a], Darrell Gaydosh[b], Santo Padula II[a], Anita Garg[c], Tiffany Biles[b], and Michael Nathal[a]
[a]NASA Glenn Research Center, 21000 Brookpark Rd., Cleveland, OH 44135
[b]OAI/NASA Glenn Research Center, 21000 Brookpark Rd., Cleveland, OH 44135
[c]University of Toledo/NASA Glenn Research Center, 21000 Brookpark Rd., Cleveland, OH 44135

ABSTRACT

The microstructure, transformation temperatures, basic tensile properties, shape memory behavior, and work output for two (Ni,Ti)Pt high-temperature shape memory alloys have been characterized. One was a $Ni_{30}Pt_{20}Ti_{50}$ alloy (referred to as 20Pt) with transformation temperatures above 230 °C and the other was a $Ni_{20}Pt_{30}Ti_{50}$ alloy (30Pt) with transformation temperatures above 530 °C. Both materials displayed shape memory behavior and were capable of 100% (no-load) strain recovery for strain levels up to their fracture limit (3-4%) when deformed at room temperature. For the 20Pt alloy, the tensile strength, modulus, and ductility dramatically increased when the material was tested just above the austenite finish (A_f) temperature. For the 30Pt alloy, a similar change in yield behavior at temperatures above the A_f was not observed. In this case the strength of the austenite phase was at best comparable and generally much weaker than the martensite phase. A ductility minimum was also observed just below the A_s temperature in this alloy. As a result of these differences in tensile behavior, the two alloys performed completely different when thermally cycled under constant load. The 20Pt alloy behaved similar to conventional binary NiTi alloys with work output due to the martensite-to-austenite transformation initially increasing with applied stress. The maximum work output measured in the 20Pt alloy was nearly 9 J/cm^3 and was limited by the tensile ductility of the material. In contrast, the martensite-to-austenite transformation in the 30Pt alloy was not capable of performing work against any bias load. The reason for this behavior was traced back to its basic mechanical properties, where the yield strength of the austenite phase was similar to or lower than that of the martensite phase, depending on temperature. Hence, the recovery or transformation strain for the 30Pt alloy under load was essentially zero, resulting in zero work output.

Keywords: high-temperature shape memory alloy, NiTi, NiPtTi, tensile properties, work output, shape memory effect, transformation strain, transformation temperatures, differential scanning calorimetry

1. INTRODUCTION

There is a growing interest in developing compact actuators and various smart systems in order to improve the efficiency and reduce emissions of aeronautic turbomachinery. A primary candidate for use in such applications is a class of materials known as shape memory alloys (SMA). Shape memory alloys are rather unique materials that have the ability to recover deformation introduced at low temperature by heating above a given transformation temperature. When this recovery process is not impeded by an external force it is an unconstrained, or free, recovery that can result in rather large changes in strain. However, this recovery process also can be "harnessed" as a source of work by having the material recover against an applied force. The classical example of this situation is to hang a weight from a shape memory alloy wire (or spring). The weight acts as a force to deform the wire while it is in the martensitic (low-temperature) condition. But when the wire is heated, it will contract as it returns to its original austenitic shape, lifting the weight by some distance. In this situation, the amount of work performed by the SMA as it transforms from the martensite to the austenite phase would be the product of the force multiplied by the distance traveled by the weight.

Conventional NiTi alloys are well known for their high work output[1,2]. In fact, SMA elements have a higher energy density than pneumatic actuators or D.C. motors and are equivalent in performance to hydraulic actuators while maintaining a much more compact footprint[3,4]. Compared to other systems such as thermostat metals, magnetic solenoids, and wax actuators, SMA actuators also produce a larger stroke in relation to their weight. Other advantages of

solid state actuators compared to hydraulic, pneumatic, and motor driven systems, are the reduction in total part count, ease of inspection, and overall reduction in inspection requirements. Shape-memory actuators are also frictionless creating a quiet, clean, and smooth motion. Of course the reduced weight of SMA actuators compared to non-solid state systems is also a major benefit in weight critical applications such as jet turbine engines and other aerospace related components.

Conventional NiTi SMA are limited primarily to applications near room temperature with maximum operating capability near 100 °C. The demand for higher-temperature versions of these conventional shape memory alloys is being driven in part by NASA's desire to develop intelligent propulsion systems, enabling designers to meet future aircraft efficiency, emissions, and noise goals. In fact, systems throughout the engine have been identified and many redesigned for possible incorporation of high-temperature shape memory alloys (HTSMA). These include adaptive (variable area/geometry) high-speed inlets, acoustic liners, shape changing blades, articulating vanes, various flow control devices, variable area bypass nozzles, fuel nozzles and mixers, active clearance control devices for the compressor and turbine sections of the engine, adaptive core exhaust chevrons, vectored or variable area exhaust nozzles, self damping components and clamps, adaptive seals, and the simple replacement of conventional actuators throughout the engine with smaller and lighter solid-state systems.

Yet as is often the case, materials development has seriously lagged component design. To date, little or no work has been done to specifically identify and develop HTSMA with optimum work characteristics for use in turbine engines and other high-temperature environments. Since NiTi alloys are superior to any other shape memory materials in terms of mechanical properties and work capability, the most practical approach to developing a high temperature actuator material would be through the introduction of ternary alloying additions to NiTi. Additions of Pd, Pt, Au, Hf, and Zr at levels greater than 10 at.% have been shown to increase the transformation temperature of NiTi alloys[5-8]. However, with the exception of research performed on NiTiHf thin films[9], the shape memory behavior (strain recovery) of all these ternary-NiTi-based alloys has been determined only under no-load or free recovery conditions, e.g., references 5,7,8,10. Therefore, the potential to use these ternary alloys as solid-state work production devices is an open question. Given the fact that work output has not been determined for any of these systems and the general lack of mechanical data, especially for the (Ni,Pt)Ti and (Ni,Au)Ti alloys, we have initiated a program to investigate the mechanical behavior of potential HTSMA in order to specifically identify compositions for high-temperature actuator applications. In this paper, we report initial properties for two compositions within the (Ni,Pt)Ti system. While both alloys display conventional shape memory behavior under no-load conditions, they display completely disparate work behavior.

2. MATERIALS AND PROCEDURES

2.1 Material Processing and Characterization

Two basic alloy compositions within the ternary NiTiPt system (always identified in atomic percent) were investigated: a $Ni_{30}Pt_{20}Ti_{50}$ alloy (referred to as 20Pt) and a $Ni_{20}Pt_{30}Ti_{50}$ alloy (30Pt). Ingots of both alloy compositions were prepared by vacuum, non-consumable-arc melting of high-purity starting components (99.95 Ti, 99.995 Pt, 99.98 Ni). Since there is a large density difference between the three elements, the initial buttons were flipped and remelted several times in order to insure complete melting and mixing of the constituents. The buttons were then drop cast into a 12.7 mm diameter copper mold. In addition, a 30Pt alloy ingot was also produced by vacuum induction melting of the same elemental constituents using a graphite crucible and cast into a 25.4 mm diameter copper mold. All cast ingots were homogenized in vacuum at 1050 °C for 72 h. The ingots were then placed into mild steel extrusion cans and extruded at a 7:1 reduction ratio. The arc melted ingots (20Pt and 30Pt (Ext7)) were extruded at 1100 °C and the induction melted ingot (30Pt (Ext19) was extruded at 900 °C.

Chemical composition was determined for all materials, after homogenization of the castings and after extrusion, by inductively coupled plasma spectroscopy and conventional N/O and C/S determination. Since there was no difference in the analyses of the cast and homogenized material before and after extrusion only the composition of the extruded material is shown in Table 1.

While work output data for conventional NiTi shape memory alloys exist in the older literature, determined primarily by measuring the recovery of deadweights on NiTi wires[1,2], we wanted to test a conventional alloy under identical

thermomechanical conditions to those that the (Ni,Pt)Ti alloys were tested. For this reason, a conventional binary NiTi alloy was purchased from Nitinol Devices Corporation, Fremont CA., as 9.63 mm diameter straightened rod referred to by Nitinol Devices as "SM495 NiTi." This material is a binary alloy suitable for shape memory applications with transformation temperatures greater than 60 °C and is used as a baseline conventional NiTi alloy in this study. The composition of the alloy is included in Table 1.

Table 1: Chemical Compositions of the Extruded Shape Memory Alloys (at.%)

Alloy ID	Ti	Ni	Pt	C	O	N
20Pt (Ext8) (arc melted precursor)	49.8	30.0	19.6	0.10	0.30	0.10
30Pt (Ext7) (arc melted precursor)	49.6	20.2	29.8	0.12	0.21	0.07
30Pt (Ext19) (induction melted precursor)	49.4	20.0	29.8	0.58	0.19	0.02
SM495 NiTi	49.9	49.9	--	<0.02	0.15	0.01

The extruded NiTiPt alloys and SM495 NiTi rod were machined into round dogbone tensile samples. The total length of each sample was 50.80 mm with threaded button ends. The gage section of each of the tensile samples was 17.4 mm long by 3.81 mm diameter. After machining, the tensile samples were annealed at 700, 440, or 300 °C, for the 30Pt, 20Pt, and SM495 NiTi alloys, respectively, for 1 hour followed by furnace cooling. After their respective heat treatments, the transformation temperatures for the Pt-containing alloys were determined by differential thermal analysis (DTA) and for the binary NiTi alloy by differential scanning calorimetry (DSC). The results are listed in Table 2.

Table 2: Transformation Temperatures (°C)

Alloy ID	A_s (°C)	A_f (°C)	M_s (°C)	M_f (°C)	Hysteresis (A_f-M_s) (°C)	Technique
20Pt (Ext8)	271	297	266	232	31	DTA
30Pt (Ext7)	594	615	560	534	55	DTA
30Pt (Ext19)	568	597	562	529	35	DTA
SM495 NiTi	51	64	61	47	3	DSC

Samples from each extrusion were also mounted, metallographically polished, and examined by SEM/EDS to characterize the basic microstructure of the alloy and to obtain an indication of the volume fraction and type of second phases present. A JEOL 840 SEM equipped with a Kevex detector was used for this purpose. All samples were analyzed in the heat treated condition.

2.2 Mechanical Testing

Mechanical testing was performed on a MTS servo-hydraulic test frame equipped with a MTS 458 controller and McGaw Technology Inc. TestExpress control software. MTS 646.10B hydraulic collet grips with a modified 680 LCF grip set were used to grip the threaded specimens. A 20 kip load cell was used, and strain measurements were taken with a 12.7 mm gage length, MTS Model 632.51B-04 extensometer, having a maximum range of +20/-10 % strain, which was equipped with 85mm long quartz probes with a v-chisel edge. Specimens were induction heated using an

Ameritherm Novastar 7.5 power supply. Cooling during thermal cycling was assisted with a high flow, 120mm, 120V muffin fan, which was only used at temperatures below the martensite finish temperature (M_f).

Prior to mechanical testing, and following heat treatment, each specimen was polished with 600 grit SiC paper to remove any oxide layer. Three type K thermocouples were spot welded to the sample, located at the middle and each end of the gauge section. Temperature gradients across the gauge were within +/-0.5% of the test temperature. Tensile specimens were strained to failure in strain control at a rate of 1×10^{-4} sec^{-1}. If a specimen reached the 20% limit of the extensometer, the test was stopped, and the specimen was unloaded.

For unconstrained strain recovery tests, specimens were deformed in tension in strain control at a rate of 1×10^{-4} sec^{-1} to the required strain level at room temperature. At this point the controller was switched to load control and the load was reduced to 0 N. Load was held at 0 N while the specimens were thermally cycled to a temperature in the range of 50 – 100 °C above the austenite finish temperature. Heating rates were maintained at 0.5 °C/sec, and the cooling fan was only activated when the sample temperature was well below the martensite finish temperature.

For constant load, strain versus temperature tests (referred to as load-bias tests), specimens were strained at room temperature to the required load in strain control at a rate of 1×10^{-4} sec^{-1}. At this point the controller was switched to load control to maintain the desired load. Specimens were then thermally cycled twice from room temperature to about 100 °C above the austenite finish temperature. Heating rates were maintained at 0.5 °C/sec and the cooling fan was only activated when the sample was well below the martensite finish temperature, and was turned off prior to the next heating cycle. Where load bias tests were run in a series of increasing loads on the same sample, the specimen was unloaded at room temperature and then strained again to the next higher load level, at which point the thermal cycling process was repeated. The work output of the SMA was determined by measuring the resultant change in strain during the martensite-to-austenite transformation during the second heating cycle and multiplying by the stress applied during the thermal cycle.

3. EXPERIMENTAL RESULTS

3.1 Microstructural Characterization

The general microstructures of the (Ni,Pt)Ti and binary NiTi alloys investigated in this study are shown in Figure 1. All the alloys were martensitic at room temperature and predominantly single phase containing a small volume percent of second phase particles. There were two types of second phases present, an intermetallic phase containing Ti, Ni and Pt and the other containing a high amount of Ti tied to the interstitials, C and O. The former is the $Ti_2(Ni,Pt)$ phase which is isostructural to the Ti_2Ni phase commonly observed in NiTi alloys[11]. The latter is an interstitial based titanium carbide or titanium oxide phase. Both types of phases were observed in the arc melted and extruded 20Pt (Ext8) and 30Pt (Ext 7) alloys and the binary SM495 NiTi (Figs. 1(a), 1(b), 1(d), respectively), but the induction melted and extruded 30Pt (Ext 19) alloy had only the interstitial containing Ti phases and no $Ti_2(Ni,Pt)$ (Fig. 1(c)). This is probably due to the fact that the induction melted and extruded 30Pt alloy contained at least five times more carbon than the other three alloys, thus tying up the excess Ti as TiC rather than forming the $Ti_2(Ni,Pt)$ phase. The carbide particles ranged in size from about 0.5 to 2 μm in the 30Pt (Ext19), while the interstitial based second phase particles in the 30Pt (Ext7) material were closer in size to 0.5 μm. The $Ti_2(Ni,Pt)$ particles in the arc melted and extruded 20Pt and 30Pt alloy and the binary NiTi were blocky in morphology and ranged from 3-10 μm in size. The total volume fraction of second phase particles was less than 2% in each of the four alloys.

3.2 Isothermal Stress-Strain Behavior

Representative stress strain curves at various temperatures for the 30Pt (Ext7) and (Ext19) materials are shown in Figure 2. The room temperature ductility of Ext7 is very similar to that reported by Lindquist and Wayman and Hosoda et al.[12] for a $Ni_{20}Pt_{30}Ti_{50}$ alloy, while Ext19 has over twice the tensile ductility of these other materials. The reason for the higher tensile ductility is not known, though 2-3 samples were tested at room temperature for each material and the results were consistent. It is possible that because of the lower extrusion temperature, Ext19 has maintained more of a wrought structure, resulting in better ductility. But at 4%, the tensile ductility of 30Pt (Ext19) is still quite low compared to conventional NiTi alloys.

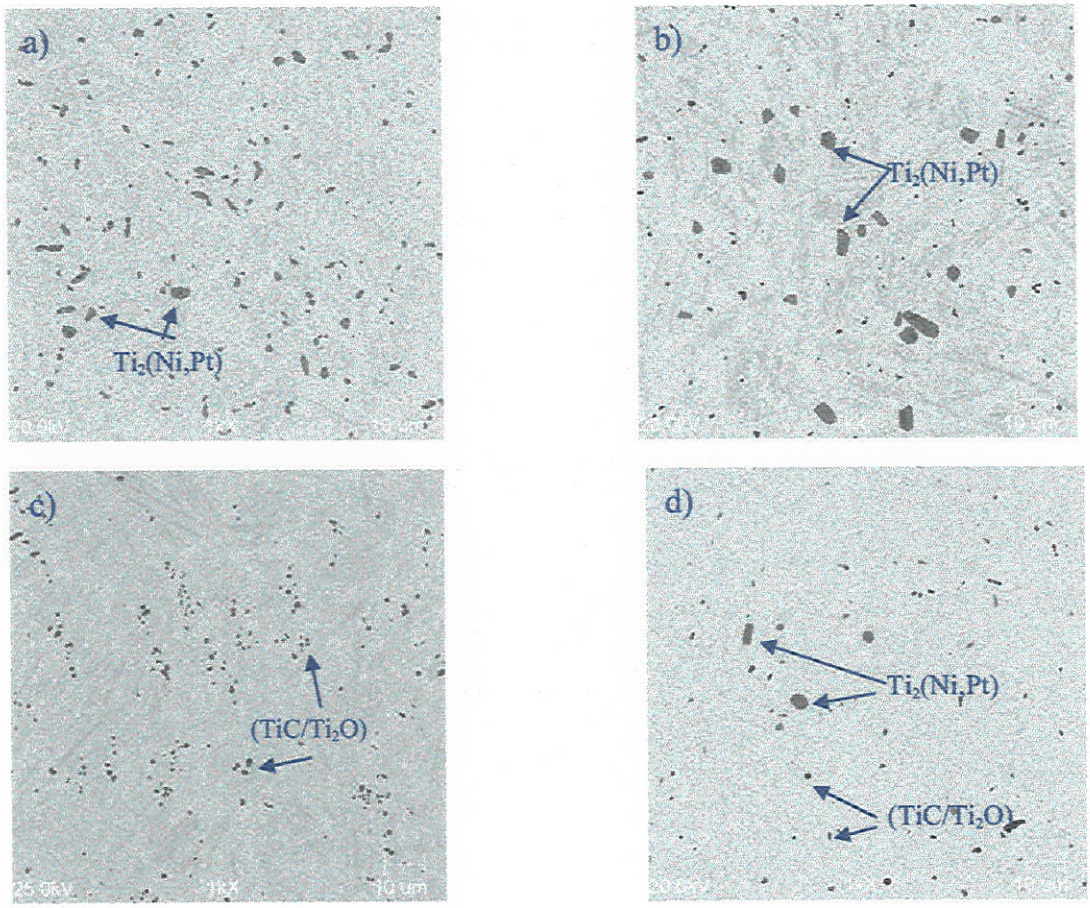

Figure 1. Backscattered electron images of the microstructures of the four alloys investigated in this study (a) 20Pt (Ext8), (b) 30Pt (Ext7), (c) 30Pt (Ext19), and (d) the binary SM495 NiTi alloy.

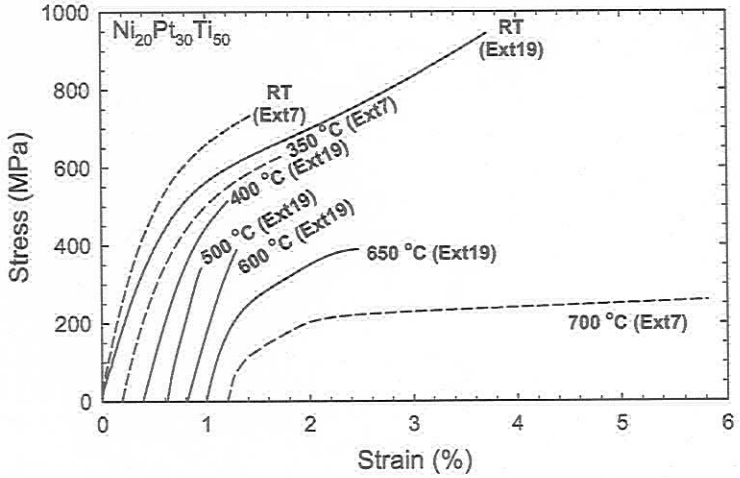

Figure 2. Representative stress-strain curves at various temperatures for the 30Pt materials. Dashed lines are 30Pt (Ext7) and solid lines are for 30Pt (Ext19). Note that tensile curves for temperatures above RT are offset from the origin.

As the test temperature increases in the 30Pt alloys, the tensile ductility of the martensite phase actually decreases. This is most readily apparent in Ext19, with a minimum in tensile ductility occurring at temperatures between 450 and 550 °C, which is still below the A_s temperature of the alloy. Therefore the ductility minimum occurs while the material is still in the martensitic condition. In this temperature range the tensile samples failed without any appreciable ductility, though at a stress level close to its anticipated yield strength. SEM examination of the fracture surfaces from samples tested within this ductility minimum and other random samples indicated that fracture always initiated at the sample surface, usually at one of the spot welds used to connect the thermocouples. As this was the case in all the alloys tested, there must be an inherent, but as yet unknown, factor contributing to the actual embrittlement of the martensite phase in the 30Pt material at these temperatures.

Above the A_f temperature of the 30Pt alloys, the tensile ductility increased as the test temperature was increased. But, the yield strength of the alloy decreased continuously with increasing temperature, regardless of the structure of the alloy. No significant increase in yield strength was observed in 30Pt samples tested above the A_f temperature, as is expected in conventional NiTi SMA.

The stress strain behavior of the 20Pt alloy at various temperatures is shown in Figure 3. Like the 30Pt materials, the stress-strain curves for the martensite phase actually show continuous hardening with increasing strain and do not exhibit a plateau stress, like conventional NiTi alloys. However, unlike the 30Pt alloy, the austenite phase for the 20Pt alloy is a factor of 2-3 times stronger than the martensite phase. Also, the short plateau region observed in the 300 and 330 °C tensile curves, which is just above the A_f temperature of this alloy, is possibly an indication of stress-induced martensite formation. If true, this would indicate that the 20Pt alloy is capable of at least limited superplastic behavior, but this would need to be confirmed.

Finally the stress strain behavior for the SM495 NiTi alloy is shown Figure 4. This figure shows the classic stress-strain response of a conventional shape memory alloy[13]. The two low-temperature curves display a distinct plateau, indicative of deformation by detwinning, followed by a linear region of increased hardening due to elastic deformation of the detwinned martensite, and a final nonlinear region due to deformation by slip. The 140 °C tensile curve also exhibits a plateau, in this case, indicative of stress-induced martensite formation, while testing at higher temperature results in behavior typical of the deformation of the austenite phase by slip. Overall, the austenite yield strength is nearly a factor of 5-10 times that of the martensite.

The tensile yield strength versus temperature behavior for all the materials is compared in Figure 5. It is clear that both the SM495 NiTi and 20Pt alloys show a very distinct and significant increase in yield strength as the temperature increases through the martensite-to-austenite transformation temperatures for each alloy. The 30 Pt alloy does not show this behavior and instead, the austenite phase has similar or lower yield strength, depending on temperature, than the martensitic form of the 30Pt alloys. Also worth noting is that the yield strength of the martensite phase in the 30Pt alloy is significantly greater than the martensite phase of either the binary NiTi or the 20Pt alloy.

3.3 Shape Memory Behavior

Shape memory behavior is the ability of a material to recover twinning-induced deformation, introduced in the martensite phase, by heating through the transformation temperature of the alloy into the austenite phase. In this case, the change in strain back to the samples original shape takes place in an unconstrained condition. Both the 20Pt and 30Pt alloys were capable of recovering all the tensile strain introduced into the sample at room temperature, between elastic and shape memory recovery, up to the fracture strain limit of the alloy. In other words, the 20Pt and 30Pt materials were capable of 100% strain recovery for total strains up to 3-4%. This behavior is shown in the stress-strain-temperature plot for the 30Pt (Ext19) alloy in Figure 6. The 30Pt (Ext7) and 20Pt alloys displayed similar behavior. Due to the limited ductility of the Pt-containing alloys, the maximum strain that these materials could completely recover could not be determined, since tensile fracture of the samples occurred at fairly low strains, both at room temperature and for any temperature below the A_s. In contrast, the binary NiTi alloy is capable of 100% recovery of up to approximately 8% total strain after tensile deformation at room temperature.

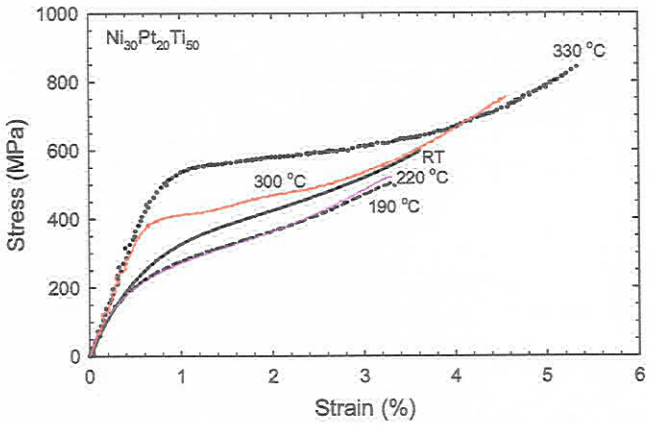

Figure 3. Representative stress-strain curves at various temperatures for the 20Pt alloy.

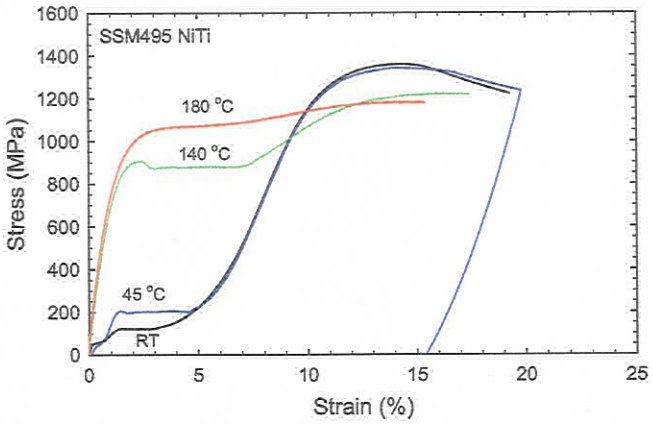

Figure 4. Representative stress-strain curves at various temperatures for the binary SM495 NiTi alloy.

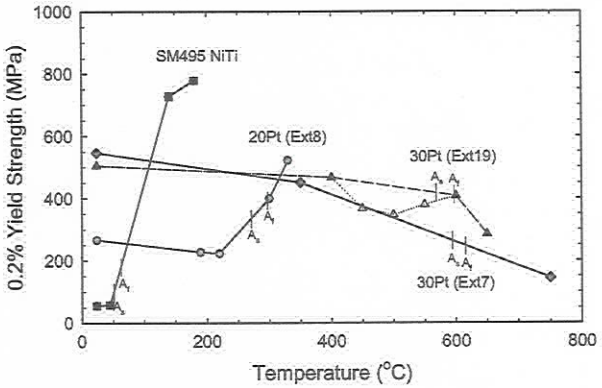

Figure 5. Tensile yield strength as a function of temperature for the materials studied. Corresponding austenite start (A_s) and austenite finish (A_f) temperatures are indicated for each alloy. Note that the open triangles for the 30Pt(Ext19) alloy represent fracture strengths since tensile failure preceded yielding at these temperatures.

3.4 Constant-Load, Strain-Temperature Tests and Work Output

Under constant-load, strain-temperature testing, the load was applied to the sample at room temperature and then the sample was both heated and cooled through the transformation temperatures while under load. During this process, the strain in the sample due to the initial applied load at room temperature, prior to thermal cycling, was usually much smaller than when the sample was cooled through the martensite temperature to room temperature under load. As a result, the transformation strain during the initial heating cycle was also much smaller than in successive cycles. This behavior is clearly demonstrated in Figure 7, which shows the initial loading and then two complete heating and cooling cycles for the 20Pt alloy under a stress of 80 MPa. While this type of behavior is quite common in conventional NiTi alloys its origin is still unknown. However, there are probably several contributing factors, at least in the case of the 20Pt alloy. 1) The yield strength of the martensite phase tends to decrease with increasing temperature, though this would be expected to contribute to the increased strain only at very high stress levels. 2) The dynamic Young's modulus for the martensite phase for the 20Pt alloy decreases significantly with increasing temperature from approximately 84 GPa at room temperature to about 68 GPa at its minimum at the A_s temperature[14]. 3) It is also possible that cycling through the transformation temperature under load begins to "train" the SMA, resulting in a greater fraction of favorably oriented martensite variants that can accommodate a larger strain in the sample for a given stress.

Regardless of the mechanism responsible for this behavior, it should be noted that this type of behavior is actually advantageous in terms of actuator applications, since smaller loads can be used to reset an actuator by cooling under load than would be required if the actuator were to be reset at room temperature.

Because of this difference in the level of strain developed in the material during loading at room temperature versus cooling through the transformation temperature under load, the first complete heating and cooling cycle at each stress level in the load-bias tests were ignored and only the second complete cycle or hysteresis is plotted in Figures 8 – 10 and used to determine the work output of the SMA (Figure 11). Representative strain-temperature hysteresis curves for the 20Pt alloy are shown in Figure 8. In this case, the transformation strain on heating increased with increasing load and a maximum work limit was reached when the sample prematurely failed on cooling under a stress of 336 MPa. Ultimately, this material could be capable of much greater work output if its tensile ductility is improved, which could be accomplished through any number of conventional metallurgical techniques, such as grain refinement, additional wrought processing, or alloy development.

In general, the work output for conventional NiTi alloys, peaks at some stress level. This is due to competing factors, in that eventually stresses become large enough to prevent complete recovery during the heating transformation, limiting the transformation strain. Therefore, even though the applied stress is increasing, the transformation strain begins to decrease and the product of the applied stress and transformation strain, which is work output, reaches a maximum at some stress level. This behavior is partially demonstrated in the strain-temperature curves for the SM495 NiTi alloy shown in Figure 9, which show a decreasing transformation strain at the highest stress levels tested. It is expected that further increases in the bias stress would result in even more significant decreases in transformation strain and thus an eventual decrease in work output. For comparison purposes, the work output of several other conventional NiTi alloys from the literature showing a more clearly defined peak in work output with increasing stress also are shown in Figure 11.

Even though the 30Pt alloy is capable of unconstrained shape memory behavior, the load-bias test results for the 30Pt alloy are completely different from those of the 20Pt and binary NiTi alloys (Figure 10). In this case, stresses below about 200 MPa are incapable of plastically deforming the martensite phase and, thus, there is no strain to recover during the transformation from martensite-to-austenite. Therefore, no work can be done by the transformation. However, these stress levels are high enough to plastically deform the austenite phase at the highest temperatures of the test cycle. Consequently, the hysteresis loops do not close. Furthermore, stress levels sufficient to deform the martensite phase (greater than about 200 MPa) are high enough to completely suppress the transformation strain during heating and are close to the yield strength of the austenite phase even near the transformation temperature, resulting in even larger permanent strains in the strain-temperature cycle. Consequently, the work output for the 30Pt alloy at any stress level is essentially zero (Figure 11), because in all cases the transformation strain is essentially zero.

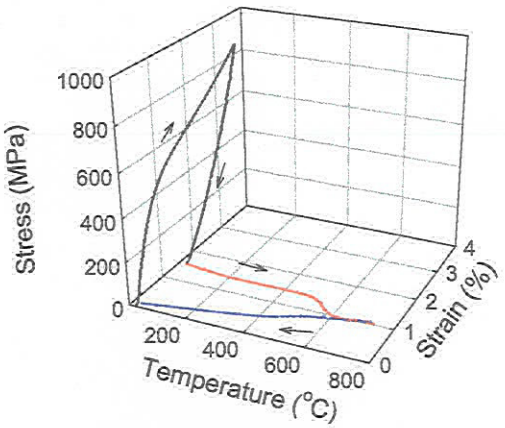

Figure 6. Shape memory, stress-strain-temperature, behavior for the 30Pt (Ext19) alloy. All room temperature induced tensile strain is recovered between elastic and shape memory recovery.

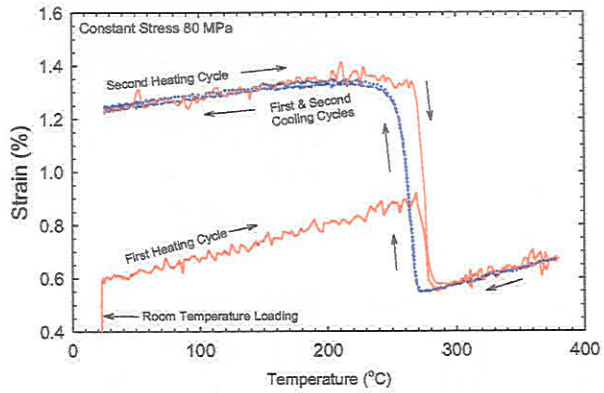

Figure 7. Initial loading and first two complete constant stress (80 MPa), strain-temperature loops for the 20Pt alloy. Heating cycles are represented by solid lines and the first and second cooling cycles by dashed and dotted lines, respectively.

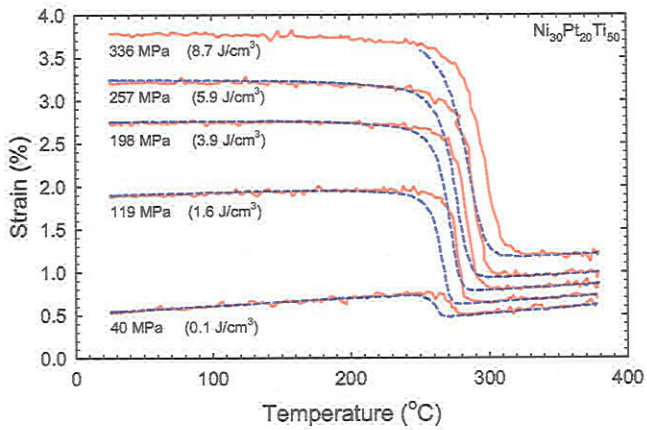

Figure 8. Load biased, strain-temperature response of the 20Pt alloy at different stress levels. Solid lines are heating curves and dashed lines are cooling curves. The constant stress level and resulting work output are indicated for each set of curves.

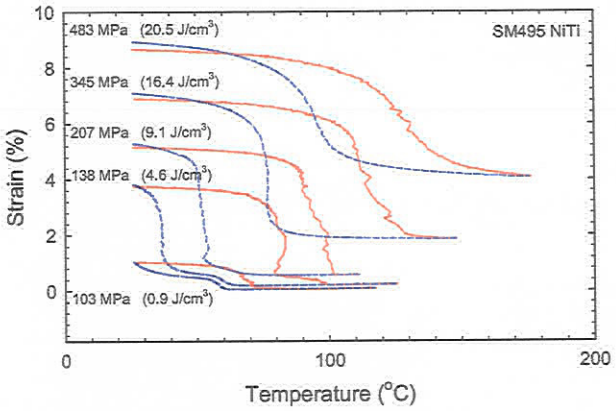

Figure 9. Load biased, strain-temperature response of the SM495 NiTi alloy at different stress levels. Solid lines are heating curves and dashed lines are cooling curves. The constant stress level and resulting work output are indicated for each set of curves.

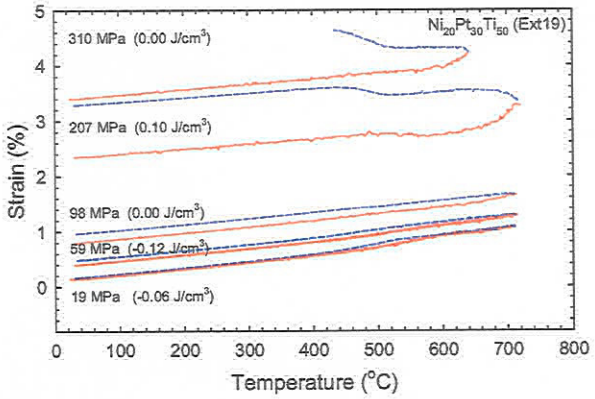

Figure 10. Load biased, strain-temperature response of the 30Pt (Ext19) alloy at different stress levels. Solid lines are heating curves and dashed lines are cooling curves. The response of the 30Pt (Ext7) material is similar.

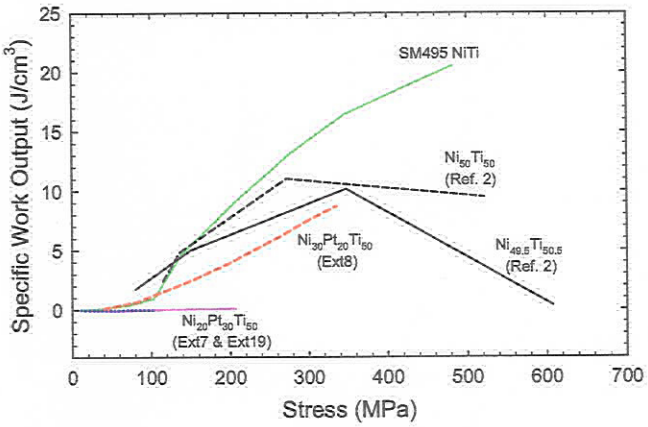

Figure 11. Comparison of the specific work output for several conventional NiTi alloys, SM495 NiTi, and the (Ni,Pt)Ti HITSMA.

4. DISCUSSION

None of the Pt-containing alloys exhibit the "classical" stress-strain behavior that is typical of NiTi alloys. Instead of a yield stress plateau with increasing strain, which is representative of easy detwinning (as shown in Figure 4 for the SM495 NiTi), the martensite stress-strain curves show continuous hardening with increasing strain and have much higher strengths than binary NiTi. Thus, deformation by detwinning is much more difficult in the ternary alloys and a clear indication of the stress at which plastic deformation by slip begins is not obvious from the stress-strain response of the material. However, given the reversible nature of the deformation induced at room temperature in both the 20Pt and 30Pt alloys, as demonstrated by unconstrained shape memory testing (e.g., Figure 6), it is apparent that deformation is occurring primarily by detwinning over the strain range investigated.

The general yield stress response of the 20Pt alloy as a function of temperature is similar to that of conventional NiTi alloys (Figure 5), with a marked increase in strength occurring as the alloy transforms from martensite to austenite with increasing temperature. This is not the case for the 30Pt alloy, with the strength of the austenite phase similar or less than that of the martensite phase, depending on temperature. Also, the yield strength of the martensite phase in the 30Pt alloy is much greater than the other two alloys; over an order of magnitude greater than the binary SM495 NiTi alloy and over twice as strong as the 20Pt alloy (Figure 5). These two factors: a very high martensite yield strength and low austenite strength conspire against the 30Pt alloy when trying to harness the martensite-to-austenite transformation in this alloy in order to perform work.

For the conventional NiTi alloys, work output increases, reaches a peak at a particular stress level, and then decreases with increasing applied stress (Figure 11) for reasons discussed above. Given the other similarities in behavior between conventional NiTi SMA and the 20Pt alloy, the latter alloy also would be expected to show the same kind of maximum in work output as a function of stress. However, during testing of the 20Pt alloy, the loads were found to exceed the martensite fracture strength of the alloy prior to reaching this peak work level. Consequently, anything done to increase the tensile ductility should also result in an increased work output for the 20Pt alloy. Given the fact that its work output is already commensurate with some binary NiTi alloys, the 20Pt alloy obviously has promise as a high-temperature actuator material. However, this is based on work production results derived essentially from single cycle load-bias testing. Under real actuator applications these materials would see repeated loading and thus fatigue life and "ratcheting" of the strain level with each cycle are of major concern. This ratcheting in strain level can be seen in the binary NiTi alloy load-bias curves shown in Figure 9. At the higher stress levels, the strain-temperature hysteresis curves do not meet up at the low temperature side and instead the strain level on cooling is greater than that on heating indicating permanent deformation of the martensite phase by slip. Given the higher martensite strength of the 20Pt alloy compared to binary NiTi, this material may be more resistant to ratcheting and thus have a longer cyclic life under high loads during temperature cycling, assuming that the tensile ductility can be improved.

In contrast, the 30Pt alloy exhibits almost no recoverable strain under load during temperature cycling; hence its work output is zero. This behavior can be traced back to the inappropriate difference in yield strength between the martensite and austenite phases with the martensite strength actually exceeding that of the austenite phase. Hence, stresses necessary to yield the martensite phase, already exceed the austenite strength during the transformation process and instead of recovering the deformed martensite phase, transformation under such applied stresses is sufficient to suppress the transformation strain and yield the austenite phase.

Thus, it is clear from this study that just having a high transformation temperature or even successfully exhibiting shape memory behavior under unconstrained conditions is no guarantee that a material could be used under work production conditions. Consequently, there are no screening shortcuts for determining SMA with good work output. Instead it will be necessary to assess all potential HTSMA by similar load-bias testing in order to determine the best candidate materials for high-temperature actuator applications.

Finally, the results of this study drive home several basic tenets for the design of alloys for optimized shape-memory work production characteristics. In general, it is necessary to 1) have a moderate stress for twinning of the martensite phase, 2) maximize the strength of the austenite phase, 3) maximize the difference between the yield strength of the austenite and martensite phases, and 4) have sufficient tensile ductility to take advantage of these strength differences.

5. SUMMARY AND CONCLUSIONS

In a search for high-temperature actuator materials, the mechanical and shape memory properties of two compositions within the (Ni,Pt)Ti system, $Ni_{30}Pt_{20}Ti_{50}$ and $Ni_{20}Pt_{30}Ti_{50}$, have been investigated. While both alloys display conventional shape memory behavior under no-load conditions, they display completely disparate work output capabilities, indicating that high transformation temperatures and even simple unconstrained recovery tests are inadequate for the identification of potential materials for work production devices. Of the two alloys studied, only the 20Pt alloy has any promise for use as a high-temperature actuator material, since the 30Pt alloy is incapable of performing work against any bias stress. Similar to conventional NiTi SMA, the yield strength of the 20Pt alloy increases dramatically as the material undergoes a transition from martensite-to-austenite with increasing test temperature. Also, the alloy has work output capability similar to many conventional NiTi alloys, limited at present by its poor tensile ductility. Even though these results are preliminary, the 20Pt alloy holds considerable promise as a high-temperature solid-state actuator. However, additional alloy development and optimization, along with more advanced testing are still needed to realize that potential.

ACKNOWLEDGEMENTS

The authors wish to thank Jami Olminsky for density determinations and compositional analysis; Anna Palczer for DTA analysis of the HTSMA; and Dan Scheiman for DSC analysis of the binary NiTi alloy. Fruitful discussions with Sue Draper, Orlando Rios, and Brad Lerch are greatly appreciated. Special thanks to Nichaela Noebe. This work was supported by the Intelligent Propulsion Systems Foundation Technology Subproject of the Ultra-Efficient Engine Technology Project, Carolyn Mercer/Susan Johnson manager.

REFERENCES

1. T.W, Duerig, D. Stockel, and A. Keeley, "Actuator and Work Production Devices", in *Engineering Aspects of Shape Memory Alloys*, T.W. Duerig, K.N. Melton, D. Stockel, and C.M. Wayman, eds., pp. 181-194, Butterworth-Heinemann, Boston, 1990.
2. W.B. Cross, A.H. Kariotis, and F.J. Stimler, *NITINOL Characterization Study*, NASA CR-1433, 1969.
3. C. Mavroidis, "Development of Advanced Actuators Using Shape Memory Alloys and Electrorheological Fluids," *Res. Nondestr. Eval.* **14**, 1-32, 2002.
4. J. Van Humbeeck, "Non-medical applications of shape memory alloys," *Maters. Sci. Engin.* **A273-275**, 134-148 (1999).
5. P.G. Lindquist and C.M. Wayman, "Shape Memory and Transformation Behavior of Martensitic Ti-Pd-Ni and Ti-Pt-Ni Alloys," in *Engineering Aspects of Shape Memory Alloys*, T.W. Duerig, K.N. Melton, D. Stockel, and C.M. Wayman, eds., pp. 58-68, Butterworth-Heinemann, Boston, 1990.
6. S.K. Wu and C.M. Wayman, "Martensitic Transformations and the Shape Memory Effect in $Ti_{50}Ni_{40}Au_{40}$ and $Ti_{50}Au_{50}$ Alloys," *Metallography* **20**, 359-376, 1987.
7. D.R. Angst, P.E. Thoma, and M.Y. Kao, "The effect of Hafnium content on the transformation temperatures of $Ni_{49}Ti_{51-x}Hf_x$ shape memory alloys," *J Phys IV* **5**, C8-747 to C8-752, 1995.
8. Z. Pu, H. Tseng, and K. Wu, "Martensite transformation and shape memory effect of NiTi-Zr high temperature shape memory alloys," in *Smart Structures and Materials 1995: Smart Materials*, SPIE Proc. Vol. **2441**, 171-178, 1995.
9. J. Zhang, *Processing and Characterization of High-Temperature Nickel-Titanium-Hafnium Shape Memory Thin Films*, Ph.D. Dissertation, Michigan State University, 2002.
10. D. Goldberg, Y.Xu, Y. Murakami, S. Morito, K. Otsuka, T. Ueki, and H. Horikawa, "Improvement of a $Ti_{50}Pd_{30}Ni_{20}$ high temperature shape memory alloy by thermomechanical treatments," *Scripta Metall. Mater.* **30**, 1349-1354, 1994.
11. A. Garg, unpublished research, NASA Glenn Research Center, 2004.
12. M. Hosoda, M. Tsuji, Y. Takahashi, T. Inamura, K. Wakashima, Y. Yamabe-Mitaria, S. Miyazaki, and K. Inoue, "Phase stability and mechanical properties of Ti-Ni alloys containing platinum group metals," *Maters. Sci. Forum* **426-432**, 2333-2338, 2003.
13. C.M. Wayman and T.W. Duerig, "An Introduction to Martensite and Shape Memory," in *Engineering Aspects of Shape Memory Alloys*, T.W. Duerig, K.N. Melton, D. Stockel, and C.M. Wayman, eds., pp. 3-20, Butterworth-Heinemann, Boston, 1990.
14. B. Lerch, unpublished research, NASA Glenn Research Center, 2005.